Research Square

Preprints are preliminary reports that have not undergone peer review.
They should not be considered conclusive, used to inform clinical practice,
or referenced by the media as validated information.

# Sensitivity of radiation shielding parameters to changes induced by land use in quartz-rich Neosols

**Lohane Tech**
State University of Ponta Grossa
**Vladia Correchel**
Federal University of Goiás
**Luiz F. Pires**
lfpires@uepg.br

State University of Ponta Grossa

**Research Article**

**Keywords:** Quartzarenic Neosols, Anthropogenic impact, Effective atomic number, Photon interaction, Electron density

**Posted Date:** June 8th, 2026

**DOI:** https://doi.org/10.21203/rs.3.rs-9558458/v1

**License:** This work is licensed under a Creative Commons Attribution 4.0 International License.
Read Full License

**Additional Declarations:** No competing interests reported.

# Abstract

The Legal Amazon in Brazil contains extensive Quartzarenic Neosols, sandy soils vulnerable to human activities such as vegetation burning and grazing. This study investigates how land use alters their chemical composition and evaluates the resulting impact on radiation shielding properties. Radiation attenuation was assessed using mass attenuation coefficient, molecular cross-sections, effective atomic number, and electron density. Soil samples from forest (F), grazing (G), and burned (B) systems were analyzed at different depths. Oxide composition varied significantly with land use. $SiO_2$ showed the highest variability, while $Fe_2O_3$ and $TiO_2$ increased with depth. Burned soils exhibited decreasing $SiO_2$ and increasing $Fe_2O_3$ and $Al_2O_3$, indicating alteration. Grazing soils had the highest $Fe_2O_3$ and $TiO_2$, while forest soils remained relatively stable. The mass attenuation coefficient was highest in grazing soils and lowest in burned surface layers, confirming an inverse relationship with silica. Molecular cross-section was sensitive to both depth and disturbance, whereas effective atomic number remained nearly constant (~ 10). Electron density increased slightly in burned soils. Overall, land use significantly affects soil composition and radiation attenuation, primarily through differences in $Fe_2O_3$, $TiO_2$, and $SiO_2$. Human activities, particularly burning, can alter the radiation-shielding capacity of these soils.


# 1. Introduction

The Legal Amazon region covers a vast area of Brazilian territory, including the states of Acre, Rondônia, Roraima, Amazonas, Pará, Maranhão, Amapá, Tocantins, and Mato Grosso [1]. In the eastern part of this region, predominantly young soils, such as Quartzarenic Neosols, are prominent [2]. These Neosols typically have a sandy texture and are primarily composed of quartz, which is rich in silicon oxides [3].

In the Amazon region, human interventions aimed at making soils more fertile are common. One practice involves cutting down vegetation and burning the biomass [4]. However, when soil is subjected to high temperatures, its chemical composition may change. In the mineral fraction, heat can induce structural transformations, such as the dehydration of clay minerals and changes in the crystallinity of iron and aluminum oxides [5]. Additionally, burning biomass results in ash deposition, temporarily enriching the soil with elements such as calcium (Ca), potassium (K), and magnesium (Mg).

Changes in soil resulting from human activity can directly affect this material for radiation shielding. Numerous studies have examined the potential of soil and its components as effective radiation-shielding materials [6, 7]. These components can also be combined with other materials to create more cost-effective shielding solutions [8]. One of the main advantages of soil is its abundance, ease of extraction, and effectiveness in shielding against radiation, both when used directly in the field and when incorporated into other materials.

Research on the potential of quartz-rich Neosols for radiation shielding is still limited [9, 10]. Additionally, no studies have evaluated how human activities might alter the composition of these soils or how such changes could affect their ability to shield against radiation. Despite advances in research methods, the existing literature offers limited insights into the use of underdeveloped soils for radiation attenuation.

Recent studies suggest that, beyond the traditional parameters analyzed, photon cross-sections (σ) may be particularly sensitive to changes in chemical composition, thereby enhancing the interpretive potential of these analyses [11].

Several parameters can be used to assess a material´s potential for radiation attenuation, including the mass attenuation coefficient (μ/ρ), molecular, atomic, and electronic cross-sections, the effective atomic number ($Z_{eff}$), and the electron density ($N_{el}$) [12–14]. These parameters offer detailed insights into how photons interact with multi-elemental materials. By applying principles of radiation-matter interaction, we can evaluate processes such as photon absorption and scattering, which are highly sensitive to soil elemental composition [15]. We therefore expect that potential changes in soil chemical composition may affect its shielding properties, particularly in Neosols.

Investigating the radiation attenuation parameters in Quartzarenic Neosols under various land-use systems is essential for understanding the impact of human activities on the chemical composition of these soils. Additionally, it helps us assess how changes in the use of tropical soils influence their ability to shield against radiation. Such studies are crucial because they provide valuable data on how dynamic processes within the soil affect its properties and, in turn, how photons interact with this material.

## 2. Materials and Methods

# 2.1 Experimental area and soil sampling

The experimental area was located near the municipality of Esperantina, in the state of Tocantins, at coordinates 5° 22’ 02” S, 48° 35’ 57” W and 90 m above sea level (Fig. 1). The average local precipitation is 1,500 mm/year, and the average temperature is 28.5°C. The climate is classified as Aw (Köppen), with a six-month rainy season (December to May) and a six-month dry season (June to November). The soil in the area was classified as Orthic Quartzic Neosol (RQo) according to the classification of the Brazilian Society of Soil Science (SiBCS) [16].

For this study, soil samples were collected from three different land-use types, namely: 1) land cultivated with grasses (G) (*Brachiara plantaginea*) since 1989; 2) land cleared of vegetation and subsequently burned (B), a process that began in 2009; and 3) land covered by native open forest vegetation (F), with a significant stock of above-ground biomass. The soil from this last area was used as a reference because it represents the soil's natural state. In the other two areas, anthropogenic activities (forest clearing) occurred, although there is no record of chemical soil amendment, which could have influenced the results.

To collect the soil samples, mini-trenches were dug, and soil monoliths measuring 5×20×20 cm were taken from the walls of these trenches at depths of 0–5, 5–10, 10–20, and 20–40 cm. The samples were then wrapped in plastic film for transport to the laboratory. In the lab, some of the soil monoliths were crushed to analyze their oxide composition. Three soil cores were collected at random locations within each depth layer in the mini-trenches.

## 2.2 Particle size analysis

The densimeter method was used to analyze soil particle size according to the procedures described in the Soil Analysis Methods Manual of the Brazilian Agricultural Research Corporation [17]. For the analyses, the samples were air-dried to constant weight and then crushed and passed through a 2-mm (10-mesh) sieve. After the texture analysis, the sand, silt, and clay content of the samples across layers and land uses could be determined (Table 1). The samples for all soil layers and land uses were classified as loamy sand.

Table 1
Average values for clay, silt, and sand content in the studied neosol under different land uses (grassland-G, biomass burning-B, and native forest-F) for the four analyzed layers (0–5, 5–10, 10–20, and 20–40 cm).

| Layer (cm) | Soil use | Clay (%) | Silt (%) | Sand (%) |
|---|---|---|---|---|
| 0–5 | F | 11.3 | 4.4 | 84.3 |
| | G | 11.7 | 4.3 | 84.0 |
| | B | 12.3 | 6.0 | 81.7 |
| 5–10 | F | 13.3 | 4.2 | 82.5 |
| | G | 11.3 | 4.7 | 84.0 |
| | B | 12.6 | 5.4 | 82.0 |
| 10–20 | F | 13.3 | 4.3 | 82.4 |
| | G | 12.0 | 3.9 | 84.1 |
| | B | 12.7 | 5.3 | 82.0 |
| 20–40 | F | 13.7 | 4.4 | 81.9 |
| | G | 12.3 | 3.4 | 84.3 |
| | B | 14.1 | 4.2 | 81.7 |

## 2.3 X-ray fluorescence

For wavelength-dispersive X-ray fluorescence (WDXRF) analysis, conducted using a Rigaku ZSX Primus II instrument, three samples (n = 3) were extracted from each of the monoliths for every layer. The samples were ground in a mortar and sieved through a 45-μm mesh. Approximately 0.5 g of each sample was weighed and pressed at 60 kN for one minute to create pellets. For samples that experienced burning, an additional 0.1 g of boric acid ($H_3BO_3$) was added as a binder to facilitate pellet formation, as the sandy soil texture made this process challenging.

After preparation, the samples were analyzed for their elemental chemical composition as oxides within characteristic wavelength ranges, from fluorine to uranium. Three measurements were obtained from each layer (0–5, 5–10, 10–20, and 20–40 cm) for each soil type, yielding a total of 36 samples (3 samples × 3 soil uses × 4 depths). Variations in oxide values were compared based on the measurement standard deviation.

# 2.4 Radiation shielding parameters

To determine the shielding parameters, the attenuation coefficient was first measured using the XCOM program. The XCOM program uses the chemical composition of the samples of interest as input data; based on this, it generates cross-sections for the photoelectric effect, coherent and incoherent scattering (Compton effect), and pair production [18]. Based on the cross-sections for each of the individual effects, the total mass attenuation coefficient is obtained, with both coherent and incoherent scattering, for any element, composition, and mixture, in the energy range from 1 keV to 100 GeV.

The values of the mass attenuation coefficient are used to calculate other shielding parameters, such as the molecular cross-section ($\sigma_M$):

$$\sigma_{M} = \frac{\mu}{\rho}\left(\frac{M}{N_A}\right)$$

1

where $M = \sum_i n_i A_i$ is the molecular weight of the compound, $N_A$ is Avogadro's number, $A_i$ is the atomic weight of the ith element, and $n_i$ is the number of formula units in the molecule.

The values for the atomic cross-section ($\sigma_A$) are obtained using the equation:

$$\sigma_{A} = \frac{\sigma_{M}}{\sum_i n_i}$$

2

where $\sum_i n_i$ is the total number of formula units of the compound.

The values for the electronic cross-section ($\sigma_E$) are obtained using the following equation:

$$\sigma_{E} = \frac{1}{N_A}\sum \frac{f_i A_i}{Z_i}\left(\frac{\mu}{\rho}\right)_i$$

3

where $f_i = \frac{n_i}{\sum_j n_j}$ and $Z_i$ are the fractional abundance and atomic number of the ith constituent element, and $\sum_j n_j$ is the total number of atoms present in the molecular formula.

The effective atomic number is calculated using the following equation:

$$Z_{eff} = \frac{\sigma_A}{\sigma_E}$$

4

The electron density is obtained from the equation:

$$N_{el} = \frac{\mu/\rho}{\sigma_E}$$

5

In this study, the energy of 59.5 keV — corresponding to the 241Am source — was selected. This choice was made because the 241Am radioactive source is one of the most commonly used in nuclear techniques for soil analysis [19, 20]. It is important to note that the main objective of this study is to analyze the effects of land use and soil depth on the radiation-shielding properties of a quartz-rich Neosol. Thus, the soil oxide composition data obtained by WDXRF were used to determine the radiation attenuation parameters. Each shielding parameter was calculated three times, as described earlier, allowing differences between layers and land uses to be compared using standard deviations.

## 3. Results and Discussion

# 3.1 Soil oxide composition

The results for the major oxides across different land uses and soil layers are presented in Table 2. We chose to present the major oxides because they constitute a large portion of the samples and have the greatest influence on radiation shielding parameters. Overall, the results show variations in the concentrations of $SiO_2$, $Al_2O_3$, $Fe_2O_3$, and $TiO_2$ among the different soil layers (0–5, 5–10, 10–20, and 20–40 cm) and among the F, G, and B soil land uses, with distinct patterns of vertical distribution.

Table 2
Average concentrations of the most abundant oxides in the studied neosol, determined using wavelength-dispersive X-ray fluorescence (WDXRF) analysis, under different land uses (grassland-G, biomass burning-B, and native forest-F) for the four analyzed layers (0–5, 5–10, 10–20, and 20–40 cm). The numbers in parentheses represent the standard deviation from the mean.

| **Oxide (%)** | **$SiO_2$** | **$Al_2O_3$** | **$Fe_2O_3$** | **$TiO_2$** |
|---|---|---|---|---|
| **F** | | | | |
| 0–5 cm | 64.0 | 30.1 | 2.3 | 1.7 |
| | (0.4) | (0.5) | (0.1) | (0.2) |
| 5–10 cm | 66.1 | 28.8 | 2.2 | 1.9 |
| | (2.8) | (2.3) | (0.3) | (0.1) |
| 10–20 cm | 67.0 | 28.1 | 2.1 | 1.9 |
| | (0.9) | (0.8) | (0.1) | (0.0) |
| 20–40 cm | 62.8 | 31.9 | 2.5 | 2.3 |
| | (0.1) | (0.1) | (0.1) | (0.1) |
| **G** | | | | |
| 0–5 cm | 75.1 | 17.8 | 3.5 | 1.4 |
| | (1.6) | (1.5) | (0.5) | (0.2) |
| 5–10 cm | 67.0 | 24.2 | 5.6 | 2.0 |
| | (2.7) | (2.0) | (0.5) | (0.1) |
| 10–20 cm | 79.3 | 15.6 | 3.3 | 1.5 |
| | (0.6) | (0.5) | (0.1) | (0.1) |
| 20–40 cm | 73.3 | 20.5 | 4.2 | 1.5 |
| | (3.5) | (2.6) | (0.7) | (0.3) |
| **B** | | | | |
| 0–5 cm | 89.0 | 9.1 | 0.8 | 0.6 |
| | (0.6) | (0.7) | (0.1) | (0.1) |
| 5–10 cm | 91.7 | 7.1 | 0.5 | 0.7 |

| Oxide (%) | $SiO_2$ | $Al_2O_3$ | $Fe_2O_3$ | $TiO_2$ |
|---|---|---|---|---|
| **F** | | | | |
| | (6.6) | (5.5) | (0.4) | (0.3) |
| 10–20 cm | 78.6 | 18.2 | 1.3 | 1.3 |
| | (8.8) | (7.4) | (0.5) | (0.7) |
| 20–40 cm | 67.3 | 28.3 | 1.8 | 1.9 |
| | (0.5) | (0.3) | (0.0) | (0.1) |

In the soil under F, the oxides exhibit relative stability throughout the profile. There are moderate variations in $SiO_2$, with a slight increase observed between the 10–20 cm depth compared to the 0–5 cm layer, followed by a decrease at greater depths. $Al_2O_3$ shows a decrease between the 10–20 cm layer and the 0–5 cm layer, but it increases again in the deepest layer. $Fe_2O_3$ shows virtually no variation among the different layers. $TiO_2$ exhibits a slight increase with depth, reaching a higher concentration in the deepest layer.

Under G, the soil displayed greater vertical heterogeneity, with no clear trend observed for $SiO_2$ concentrations. The highest level of $SiO_2$ was recorded at a depth of 10–20 cm. $Al_2O_3$ showed variations that depended on depth, with higher values found at 5–10 cm and lower values at 10–20 cm. $Fe_2O_3$ peaked in the 5–10 cm layer, indicating a vertical redistribution. Meanwhile, $TiO_2$ remained relatively stable, with a slight increase noted at the 5–10 cm layer.

In the soil under B, the trends observed along the profile are more pronounced. $SiO_2$ tends to decrease with depth, while $Al_2O_3$ and $Fe_2O_3$ progressively increase, suggesting that this land-use practice has impacted the chemical composition of the soil. $TiO_2$ displays the most consistent pattern among the elements, showing a continuous increase throughout the profile. These findings indicate that the effects of burn management extend beyond the surface, influencing subsurface layers and altering the distribution of oxides across different soil particle size fractions.

When comparing land uses, B exhibits higher $SiO_2$ contents in the surface layers, F shows the lowest values, and G exhibits greater variability. In general, land use affected $SiO_2$ content across the different layers. For $Al_2O_3$, F tends to have higher surface values, while B stands out for its increase with depth. Again, in general, the land uses presented differences across layers. $Fe_2O_3$ was higher for land use G in all layers compared to F and B, especially in the intermediate layer, while B showed a lower surface concentration that increased with depth. $TiO_2$ exhibits similar behavior across land uses, with a general trend of increasing with depth.

In general, $TiO_2$ and $Fe_2O_3$ exhibit the most consistent trends of variation throughout the profile, with increases with depth across all land uses. $Al_2O_3$ also tends to concentrate in the deeper layers overall,

especially in B, while $SiO_2$ shows greater dependence on land use and greater variability. These results indicate that pedogenic processes and different land uses jointly influence the vertical redistribution of oxides in the soil [21].

It is worth mentioning that Neosols are characterized by their poor weathering, which means that the relationship between silica ($SiO_2$) and the oxides of aluminum (Al) and iron (Fe) reflects an early stage of soil formation [22]. In this stage, secondary phases develop only to a limited extent, helping stabilize the soil structure. Functionally, the reduction of oxides such as aluminum oxide and iron oxide, which are associated with the clay fraction and the formation of cementing agents, can influence radiation attenuation in soil structure [23]. However, this aspect was not explored in our study. Additionally, the relatively high silica concentrations reinforce the predominance of sandier, less reactive soil fractions.

When the measured oxides are analyzed, the values obtained are consistent with the literature for soils [24, 25]. However, variations are expected depending on the source material and environmental conditions. Finally, the high standard deviations observed for some oxides are attributed to granulometric heterogeneity and the presence of organic matter [21], especially in B, which hinders homogenization during sample preparation.

# 3.2 Mass attenuation coefficient

The mass attenuation coefficient was simulated based on the composition of soil oxides (Table 2) using the XCOM program, which is commonly used in radiation shielding studies [23, 24, 26–30]. Table 3 shows the μ/ρ values for the equivalent photon energy of a $^{241}Am$ source.

Table 3
Average values of the mass attenuation coefficient (μ/ρ) simulated using the XCOM program for the photon energy of 59.5 keV for the Neosol studied under different land uses (grassland-G, biomass burning-B, and native forest-F) for the four analyzed layers (0–5, 5–10, 10–20, and 20–40 cm).

| **μ/ρ ($cm^2\ g^{-1}$)** | | | | |
|---|---|---|---|---|
| Soil layer | 0–5 cm | 5–10 cm | 10–20 cm | 20–40 cm |
| F | 0.274 | 0.273 | 0.272 | 0.274 |
| | (0.001) | (0.001) | (0.001) | (0.001) |
| G | 0.287 | 0.298 | 0.280 | 0.286 |
| | (0.001) | (0.002) | (0.001) | (0.003) |
| B | 0.260 | 0.259 | 0.267 | 0.270 |
| | (0.002) | (0.003) | (0.004) | (0.001) |

In the surface layer (0–5 cm), G showed a relative difference in μ/ρ compared to F of c. +4.7%. This layer had the highest concentrations of $Fe_2O_3$ and $TiO_2$, which directly influence μ/ρ [31]. A similar trend was

observed in the 5–10 cm layer, where G exhibited a μ/ρ value c. 9.2% higher than that of F, again due to elevated concentrations of iron and titanium oxides. In contrast, B displayed the lowest μ/ρ values in the upper layers, being c. 5% lower than those of F. This difference is mainly attributed to the higher $SiO_2$ content in B in the upper layers, highlighting how silica composition affects μ/ρ [9, 31].

In the 10–20 cm layer, G exhibited a μ/ρ value c. 2.9% higher than F, and c. 4.9% higher than B. At this depth, the highest concentration of $SiO_2$ is also observed in G, approximately 12% higher than in F, reinforcing the inverse relationship between the increase in this oxide and the μ/ρ values [28, 32]. The lowest μ⁄ρ value was observed in B (c. 1.8% lower than in F), a finding primarily explained by lower concentrations of $Fe_2O_3$ and $TiO_2$ [33]. In the deepest layer analyzed (20–40 cm), the trend in μ/ρ was the same as in the upper layers. The soil under G exhibited the highest μ/ρ value, exceeding c. 4.4% compared to F and c. 5.9% compared to B.

In general, the highest μ/ρ values were observed in G across all analyzed layers (0–5, 5–10, 10–20, and 20–40 cm). This result is attributed to the higher concentrations of $Fe_2O_3$ and $TiO_2$ present in this soil use, as their molar masses ($Fe_2O_3$ = 159.69 g $mol^{-1}$; $TiO_2$ = 79.87 g $mol^{-1}$) contribute to increased photon attenuation. Conversely, a trend of decreasing μ/ρ with increasing $SiO_2$ concentration (60.08 g $mol^{-1}$) was noted, indicating an inverse relationship between this oxide and μ/ρ [34]. Additionally, $Al_2O_3$ (101.96 g $mol^{-1}$) had a secondary influence, likely due to the similarity of its effective atomic number to that of $SiO_2$ [18].

In the surface layers (0–5 and 5–10 cm), B exhibited more significant differences compared to F. However, in the deeper layers (10–20 and 20–40 cm), the μ/ρ values tended to converge. This pattern can be explained by a decrease in $SiO_2$ concentration and a relative increase in $Fe_2O_3$ and $TiO_2$ as depth increases, indicating a mineralogical redistribution throughout the soil profile [21].

Figure 2 shows trends in μ/ρ variation, along with those in the combined variation of $Fe_2O_3$ and $TiO_2$ oxides. Overall, since Fe and Ti are the heaviest elements among the major oxides that constitute Neosol, they strongly influence the behavior of μ/ρ. This fact is primarily related to the dependence of μ/ρ on the photoelectric-effect cross section and incoherent scattering at the analyzed photon energy [35].

Analysis of μ/ρ across different soil layers and land uses revealed an intrinsic dependence on soil elemental composition, corroborating previous studies. Mudahar et al. [36] and Medhat [37] had already demonstrated that μ/ρ is highly sensitive to the presence of elements with high atomic numbers (Z), especially in low-energy ranges (up to c. 0.8 MeV), where samples composed of minerals containing heavy elements such as Mn, Cr, Fe, and Zr exhibit significantly higher attenuation values.

In soil analysis, recent literature confirms that iron and titanium are the main determinants of μ/ρ values. However, silicon can also play an important role when present in large quantities, as is the case in sandier soils. Pires et al. [38] confirmed that the concentrations of $Fe_2O_3$ and $TiO_2$ oxides directly influence increases in attenuation parameters. Additionally, Camargo et al. [39] observed that, in the energy range from 1 keV to 100 keV, soils with higher $SiO_2$ and $Al_2O_3$ contents exhibit the lowest μ/ρ

values, highlighting the role of light elements in reducing the probability of photon interaction with the soil matrix.

## 3.3 Molecular cross-section

The average values for the molecular cross-section for each land use and different layers for photons with energy of 59.5 keV are presented in Table 4.

Table 4
Average values of the molecular cross-section ($\sigma_M$) for the photon energy of 59.5 keV for the Neosol studied under different land uses (grassland-G, biomass burning-B, and native forest-F) for the four analyzed layers (0–5, 5–10, 10–20, and 20–40 cm).

| **$\sigma_M$ (barn/molecule)** | | | | |
|---|---|---|---|---|
| Soil layer | 0–5 cm | 5–10 cm | 10–20 cm | 20–40 cm |
| F | $5.34x10^5$ | $2.32x10^5$ | $8.77x10^5$ | $1.19x10^6$ |
| | ($6x10^4$) | ($3x10^4$) | ($8x10^4$) | ($8x10^4$) |
| G | $5.75x10^5$ | $4.41x10^5$ | $7.00x10^4$ | $2.24x10^5$ |
| | ($5x10^4$) | ($5x10^4$) | ($1x10^4$) | ($1x10^4$) |
| B | $1.34x10^5$ | $1.93x10^5$ | $1.09x10^6$ | $4.50x10^4$ |
| | ($7x10^4$) | ($5x10^4$) | ($6x10^5$) | ($1x10^4$) |

The $\sigma_M$ values exhibited a systematic variation based on depth and land use type. In F and G, differences in $\sigma_M$ were noted between soil layers. Specifically, in F, $\sigma_M$ tended to increase, while in G, it tended to decrease when comparing the surface layers to the deeper layers (Fig. 3). In B, the variation pattern was more heterogeneous, showing a maximum $\sigma_M$ value at 10–20 cm and a minimum at 20–40 cm, while the surface layers (0–5 cm and 5–10 cm) did not show significant differences from each other. Additionally, an analysis of the $\sigma_M$ values for the Neosol studied indicated that they fall within the expected range for soils with variations in oxide composition [23].

When analyzing the variation in $\sigma_M$ across layers, it is evident that, in addition to the influence of $\mu/\rho$, the molecular weight of the compound significantly affects the molecular cross-section (Fig. 3). At specific energies such as 59.5 keV (as observed with $^{241}Am$), processes like the photoelectric effect are notably dependent on the atomic number, with a relationship approximately proportional to $Z^{4-5}$ [35]. This means that the presence of heavier elements significantly affects the values of $\sigma_M$ [40].

However, in the case of Neosols, which are primarily composed of silica, it has also been noted that the atomic contribution of $SiO_2$ ($n_iA_i$) can significantly influence $\sigma_M$. Our study found that the $n_iA_i$ of $SiO_2$

follows the same trend as the total $n_iA_i$, underscoring the oxide's effect on the $\sigma_M$ values in the Neosol studied (Fig. 4). Although $SiO_2$ has the lowest molecular weight among the major oxides in the studied soil, its high abundance can strongly impact the overall molecular weight when all oxides are taken into account [23].

A comparison of soil land use at different depths showed distinct patterns (Table 4). At a depth of 0–5 cm, F and G did not differ from each other but had higher $\sigma_M$ values than B. At a depth of 5–10 cm, G exhibited significantly higher values, whereas F and B showed no difference. At the 10–20 cm depth, G had significantly lower values, again with F and B not differing from each other. Finally, at a depth of 20–40 cm, there was a clear distinction among the land uses, with values increasing in the order B < G < F, indicating a greater impact of land use in the deeper soil layers.

The observed differences suggest that $\sigma_M$ values are sensitive to structural and compositional changes in the soil induced by land use. The more uniform behavior and increase with depth in F is consistent with less disturbed systems, in which there is greater structural stability and profile organization [21]. In G, the discontinuity at 10–20 cm may reflect effects of compaction and redistribution of organic matter and minerals associated with land-use processes [41]. In B, the high variability and the peak at intermediate depth indicate strong heterogeneity, possibly resulting from practices such as burning and soil disturbance [42]. Taken together, these results show that $\sigma_M$ is a sensitive indicator of use-associated physicochemical soil modifications, making it a potentially useful parameter for radiation shielding analysis.

## 3.4 Effective atomic number

The $Z_{eff}$ results for different land uses and depths are presented in Table 5. $Z_{eff}$ is related to the average of all atomic numbers present in the soil's chemical composition [23]. For the Neosol studied, the atomic numbers ranged from 8 (O) to 41 (Nb), considering all the analyzed elements, not just the major oxides.

Table 5
Average values of the effective atomic number ($Z_{eff}$) for the photon energy of 59.5 keV for the Neosol studied under different land uses (grassland-G, biomass burning-B, and native forest-F) for the four analyzed layers (0–5, 5–10, 10–20, and 20–40 cm).

| **$Z_{eff}$** | | | | |
|---|---|---|---|---|
| Soil layer | 0–5 cm | 5–10 cm | 10–20 cm | 20–40 cm |
| F | 10.06 | 10.03 | 10.02 | 10.05 |
| | (0.01) | (0.02) | (0.04) | (0.01) |
| G | 10.08 | 10.15 | 10.06 | 10.07 |
| | (0.01) | (0.06) | (0.01) | (0.01) |
| B | 10.01 | 10.00 | 10.05 | 10.04 |
| | (0.01) | (0.01) | (0.03) | (0.01) |

Since $Z_{eff}$ depends on the inverse of $\sigma_E$, and $\sigma_E$ depends on the fractional abundance ($f_i$), the elements with the highest fractional abundance values are those present in the highest percentage in the soil's elemental composition [6]; for the land uses studied, these are Si and Al (Table 2). Therefore, the $Z_{eff}$ values were closer to the atomic numbers of these elements (Z = 13 for Al; Z = 14 for Si) [24].

The average $Z_{eff}$ values for Neosol, determined at 59.5 keV, showed little variation across the different land uses (F, G, B) and depths analyzed (0–5, 5–10, 10–20, and 20–40 cm). In general, $Z_{eff}$ values remained close to 10 under all conditions (Fig. 5). These values are consistent with those reported in the scientific literature for soils [15, 24, 30].

In the surface layer (0–5 cm), B was lower than F and G, which showed virtually no difference between them. In the 5–10 cm layer, a greater distinction was observed among land uses, with G having a significantly higher value than F and B, which showed no differences between them. For the deeper layers (10–20 and 20–40 cm), $Z_{eff}$ values did not differ among land uses. This indicates that, at greater depths, land use has a reduced influence on the effective atomic number.

Analysis of the different layers within each land use reinforces this pattern. The soil under F showed virtually constant values throughout the profile. In contrast, the soil under G showed a localized increase in the 5–10 cm layer, mainly due to higher $Fe_2O_3$ and $TiO_2$ contents in that layer (Fig. 5) [43]. On the other hand, the soil under B showed a slight increase with depth, which falls within the range of the standard deviation.

Soils with a more clay-rich particle size distribution and a chemical composition containing a higher percentage of $Fe_2O_3$ are typically characterized by higher $Z_{eff}$ values [38]. Kumar et al. [44] had already

noted that minerals with higher amounts of $Fe_2O_3$ in their composition have higher $Z_{eff}$ values compared to those with higher $SiO_2$ contents. This demonstrates $Z_{eff's}$ sensitivity to changes in the chemical composition of soils consisting mainly of elements with high atomic numbers [43, 45]. Based on this information, it is observed that $Z_{eff}$ generally follows the same trend of variation as $Fe_2O_3$ (Fig. 5).

The effective atomic number is a crucial parameter for evaluating how radiation interacts with matter, particularly at energy levels in the tens of kiloelectronvolts (keV) range, where the photoelectric effect is most significant. In this energy range, $Z_{eff}$ greatly depends on the material's elemental composition, especially the presence of elements with higher atomic numbers.

The results indicate that changes in land use, including biomass burning and pasture conversion, did not significantly affect $Z_{eff}$. This finding suggests that the dominant soil mineral constituents, which govern its radiative behavior, remain relatively stable despite these interventions [21]. From a radiation shielding perspective, the small variation in $Z_{eff}$ across different land uses and depths suggests that Neosol has relatively uniform photon attenuation within this energy range.

## 3.5 Electron density

The $N_{el}$ results for different land uses and soil layers are presented in Table 6. It is worth noting that this parameter depends on μ/ρ and $Z_{eff}$, so variations in these parameters will also influence the $N_{el}$ results [40].

Table 6
Average values of the electron density ($N_{el}$) for the photon energy of 59.5 keV for the Neosol studied under different land uses (grassland-G, biomass burning-B, and native forest-F) for the four analyzed layers (0–5, 5–10, 10–20, and 20–40 cm).

| **$N_{el}$ ($\times 10^{23}$ electron $g^{-1}$)** | | | | |
|---|---|---|---|---|
| Soil layer | 0–5 cm | 5–10 cm | 10–20 cm | 20–40 cm |
| F | 2.95 | 2.95 | 2.94 | 2.92 |
| | (0.01) | (0.01) | (0.01) | (0.01) |
| G | 2.95 | 2.95 | 2.96 | 2.94 |
| | (0.01) | (0.02) | (0.01) | (0.01) |
| B | 2.98 | 2.98 | 2.97 | 2.95 |
| | (0.01) | (0.01) | (0.02) | (0.01) |

$N_{el}$ values showed little variation across different treatments and depths, ranging from $2.92\times10^{23}$ to $2.98\times10^{23}$ electrons $g^{-1}$. However, consistent differences were observed among land uses. Generally, land use B exhibited the highest $N_{el}$ values across almost all layers, particularly in the surface layers (0–

5 and 5–10 cm), with notable differences compared to F and G. Conversely, F consistently had the lowest values, especially in the deepest layer (20–40 cm). In contrast, G displayed intermediate values. These differences were most pronounced in the surface and deep layers, with no significant differences among land uses in the 10–20 cm layer.

Regarding depth variation, a decreasing trend in $N_{el}$ values was observed in both F and B, with the greatest reduction between the surface and the deepest layers. In contrast, the values in G remained virtually constant throughout the profile, with strong overlap across all layers, indicating no significant variation. These findings suggest that land use affects not only the absolute $N_{el}$ values but also their distribution within the profile.

It can be observed that $N_{el}$ follows the same trend as $SiO_2$ oxide rather than $Fe_2O_3$. Although $N_{el}$ depends on $\mu/\rho$ and $Z_{eff}$, which in turn depend directly on the iron oxide content, $N_{el}$ values are also generally influenced by the most abundant oxide (Fig. 6) [46]. Higher $N_{el}$ values indicate a greater probability of interaction, primarily due to the photoelectric effect [35], suggesting greater shielding efficiency [24]. In this context, the higher values observed in B suggest that this system has a greater capacity for radiation attenuation compared to F and G, especially in the surface layers, where the difference is most pronounced. On the other hand, lower values in F, especially at greater depths, indicate a lower relative shielding potential.

The variations observed in land use are linked to changes in soil elemental composition, which directly affect the number of electrons per unit mass [24]. In G, a greater uniformity in $N_{el}$ values was noted, suggesting that this parameter was not affected by depth-dependent differences in soil elemental composition (Fig. 6). In contrast, the decrease in $N_{el}$ values with depth in F and B may be associated with variations in organic matter content and grain-size distribution throughout the soil profile [24]. These results indicate that land use has a measurable effect on properties relevant to soil-radiation interactions, with implications for studies of natural shielding and for the assessment of environments exposed to radioactive sources.

# 4. Conclusions

The results show that, in general, the studied Neosol exhibits variations in chemical composition across different land uses (F, G, and B), particularly in the amounts of $SiO_2$, $Al_2O_3$, and $Fe_2O_3$, with the soil under B standing out as tending to be richer in silica in the surface layers. However, when depth is taken into account, these differences become less evident.

The mass attenuation coefficient varied with the elemental composition of the samples at a photon energy of 59.5 keV. The soil under G showed the highest $\mu/\rho$ values in the surface layers (0–5 and 5–10 cm), followed by F, while B showed the lowest. In the deeper layers (10–20 and 20–40 cm), the differences between treatments decreased, mainly due to increased $Fe_2O_3$ and $TiO_2$ contents. Regarding

variation within each land use with depth, F remained practically constant; G showed greater fluctuation, with a peak in the 5–10 cm layer; and B showed a slight tendency to increase with depth.

In general, $\sigma_M$ values vary across land uses and with depth. In the surface layer (0–5 cm), only B differed from the other land uses, and in the next two layers (5–10 and 10–20 cm), only G differed. In the deepest layer (20–40 cm), however, all land uses showed differences. In summary, land use influences the distribution of $\sigma_M$, with F tending toward higher values at depth and G and B showing more pronounced variations between layers.

$Z_{eff}$ values showed little variation across land uses and depths. The greatest variations among land uses were observed in the most superficial layers (0–5 and 5–10 cm), mainly in G, with smaller differences at depth. In the analysis of $Z_{eff}$ variation with depth for a given land use, it was observed that $Z_{eff}$ remained practically stable with depth, indicating a small influence of chemical composition variations along the profile on $Z_{eff}$.

$N_{el}$ values showed relatively small variations among different land uses and depths, although consistent patterns were observed that highlight the influence of soil cover and composition. Land use B showed the highest values, especially in the surface layers, while F showed the lowest, particularly at greater depths, and G showed more uniform behavior throughout the profile. It was also observed that the distribution of $N_{el}$ correlates more strongly with variations in $SiO_2$ than with those in $Fe_2O_3$, indicating that overall soil composition, rather than a single constituent, affects $N_{el}$.

In summary, the study's results indicate that certain parameters are more sensitive than others in revealing the potential effects of land use and depth-dependent variations in soil chemical composition on radiation shielding. The findings suggest that silicon-rich soils could be an interesting alternative material for radiation shielding, especially considering the high sand content found in Neosol.

# Declarations


### Acknowledgements

The authors would like to thank the “Conselho Nacional de Desenvolvimento Científico e Tecnológico” (CNPQ) for the productive research grant (303950/2023-4) and the “Coordenação de Aperfeiçoamento de Pessoal de Nível Superior” (CAPES) for the financial support (code 001).


### Author Contributions

Lohane Tech: Investigation, Formal analysis, Data curation, Writing – original draft. Vladia Correchel: Conceptualization, Methodology. Luiz F. Pires: Conceptualization, Writing – original draft, Writing – review & editing, Supervision, Funding.


### Funding

Open access funding provided by “Coordenação de Aperfeiçoamento de Pessoal de Nível Superior” (CAPES).

**Data Availability**

Data will be made available on request.

**Ethical Approval**

Not applicable.

**Generative AI and AI-assisted technologies in the writing process**

In preparing this article, the authors utilized Grammarly, an AI-assisted tool, to enhance the manuscript’s overall readability. Following the use of this tool, the authors reviewed and edited the content as needed.

**Competing Interests**

The authors declare no competing interests.

# References

1. Becker BK (2016) Geopolitics of the Amazon. Area Dev Policy 1(1):15–29
2. da Silva Fonseca, J., César Costa Campos, M., Gomes de Brito Filho, E., Campos Mantovanelli,B., Santos Silva, L., Ferreira Leite de Lima, A., … Antônio Coutrim dos Santos, L.(2019). Soil-landscape relationship in sandstone-gneiss topolithosequence in Amazonas,Brazil. Solid Earth Discussions, 2019, 1–24.
3. Batista, E. M., Shultz, J., Matos, T. T., Fornari, M. R., Ferreira, T. M., Szpoganicz,B., … Mangrich, A. S. (2018). Effect of surface and porosity of biochar on water holding capacity aiming indirectly at preservation of the Amazon biome. Scientific Reports, 8(1), 10677.
4. Sorrensen CL (2000) Linking smallholder land use and fire activity: examining biomass burning in the Brazilian Lower Amazon. For Ecol Manag 128(1–2):11–25
5. Ketterings QM, Bigham JM, Laperche V (2000) Changes in soil mineralogy and texture caused by slash-and-burn fires in Sumatra, Indonesia. Soil Sci Soc Am J 64(3):1108–1117
6. Alsafi HM, Marashdeh MW, Tashlykov OL, Mahmoud KA (2026) Enhancing the structural, morphological, and radiation shielding properties of calcined soil using granite and boric acid. Eur Phys J Plus 141(2):190
7. Sayyed MI, Akman F, Turan V, Araz A (2018) Evaluation of radiation absorption capacity of some soil samples. Radiochim Acta 107(1):83–93
8. Akbulut S, Sehhatigdiri A, Eroglu H, Çelik S (2015) A research on the radiation shielding effects of clay, silica fume and cement samples. Radiat Phys Chem 117:88–92

9. Pires LF (2022) Radiation shielding properties of weathered soils: influence of the chemical composition and granulometric fractions. Nuclear Eng Technol 54(9):3470–3477
10. Obaid SS, Sayyed MI, Alameen AS, Gaikwad DK, Mahmoud KA (2024) Extensive analysis of several Indian and Yemeni soils' gamma-ray shielding characteristics: An experimental and simulation approach. Nuclear Eng Technol 56(9):3558–3565
11. Medhat ME, Pires LF (2016) Importance of photo atomic cross section for studying physical properties of different types of soil. X-Ray Spectrom 45(4):202–206
12. Akman F, Turan V, Sayyed MI, Akdemir F, Kaçal MR, Durak R, Zaid MHM (2019) Comprehensive study on evaluation of shielding parameters of selected soils by gamma and X-rays transmission in the range 13.94–88.04 keV using WinXCom and FFAST programs. Results Phys 15:102751
13. Obaid RM, Al-Jawdah AM, Aljarrah RM (2025) Evaluation of the Capability of Utilizing the Local Soil as a Nuclear Radiation Shielding Materials. Iraqi J Appl Phys 21(2):205–208
14. Nagaraja N, Manjunatha HC, Seenappa L, Sridhar KN, Ramalingam HB (2020) Radiation shielding properties of silicon polymers. Radiat Phys Chem 171:108723
15. Hila, F. C., Javier-Hila, A. M. V., Sayyed, M. I., Asuncion-Astronomo, A., Dicen,G. P., Jecong, J. F. M., … Amorsolo Jr, A. V. (2021). Evaluation of photon radiation attenuation and buildup factors for energy absorption and exposure in some soils using EPICS2017 library. Nuclear Engineering and Technology, 53(11), 3808–3815.
16. Dos Santos, H. D., Jacomine, P. T., Dos Anjos, L. H. C., De Oliveira, V. Á., Lumbreras,J. F., Coelho, M. R., … JOÃO BERTOLDO DE OLIVEIRA, I. A. C. (2018). Brazilian Soil Classification System.
17. EMBRAPA (1997) Manual de métodos de análise de solo. Rio de Janeiro 997:212
18. Berger MJ, Hubbell JH (1987) *XCOM: Photon cross sections on a personal computer* (No. NBSIR-87-3597). National Bureau of Standards, Washington, DC (USA). Center for Radiation Research
19. Hopmans JW, Dane JH (1986) Calibration of a dual-energy gamma radiation system for multiple point measurements in a soil. Water Resour Res 22(7):1109–1114
20. Gurler O, Tumsavas Z, Akar Tarim U (2020) Gamma-ray attenuation study for the soils of Bursa, Turkey, in the energy range 59.5–1332.5 keV. Iran J Sci Technol Trans A: Sci 44(4):1161–1166
21. Alekseev A, Alekseeva T, Kalinin P, Hajnos M (2018) Soils response to the land use and soil climatic gradients at ecosystem scale: Mineralogical and geochemical data. Soil Tillage Res 180:38–47
22. Nóbrega MT, Serra E, Silveira H, Terassi PMB, Bonifácio CM (2015) Landscape structure in the Pirapó, Paranapanema 3 and 4 Hydrographic Unit, in the state of Paraná, Brazil. Brazilian J Biology 75(4 suppl 2):107–119
23. Camargo MA, Kodum KS, Pires LF (2022) How does the soil chemical composition affect its cross-sections, effective atomic number and electron density? Computer simulation analysis to highlight the radiation-soil interaction processes. Braz J Phys 52(5):154
24. Kucuk N, Tumsavas Z, Cakir M (2013) Determining photon energy absorption parameters for different soil samples. J Radiat Res 54(3):578–586

25. Taqi AH, Khalil HJ (2017) An investigation on gamma attenuation of soil and oil-soil samples. J radiation Res Appl Sci 10(3):252–261
26. Demir L, Han I (2009) Mass attenuation coefficients, effective atomic numbers and electron densities of undoped and differently doped GaAs and InP crystals. Ann Nucl Energy 36(7):869–873
27. Kurudirek M, Özdemir Y, Türkmen İ, Levet A (2010) A study of chemical composition and radiation attenuation properties in clinoptilolite-rich natural zeolite from Turkey. Radiat Phys Chem 79(11):1120–1126
28. Medhat ME, Pires LF, Arthur RCJ (2014) Analysis of photon interaction parameters as function of soil composition. J Radioanal Nucl Chem 300(3):1105–1112
29. Singh VP, Medhat ME, Badiger NM (2014) Photon attenuation coefficients of thermoluminescent dosimetric materials by Geant4 toolkit, XCOM program and experimental data: a comparison study. Ann Nucl Energy 68:96–100
30. Ferreira TR, Pires LF, Brinatti AM, Auler AC (2018) Surface liming effects on soil radiation attenuation properties. J Soils Sediments 18(4):1641–1653
31. Tech L, Pires LF, Brinatti AM, Saab SC, Correchel V, Momoli RS (2022) Elemental and radiation attenuation parameter analyses to characterize a Cambisol from the Serra Dourada State Park, Brazil. Environ Earth Sci 81(3):63
32. Han I, Demir L, Şahin MEHMET (2009) Determination of mass attenuation coefficients, effective atomic and electron numbers for some natural minerals. Radiat Phys Chem 78(9):760–764
33. Elqahtani ZM, Alrowaili ZA, Alsaiari NS, Alnairi MM, Olarinoye IO, Al-Buriahi MS (2025) Gamma absorption and radiation shielding properties of apatite-wollastonite containing SiO2, Fe2O3, and TiO2. Radiat Phys Chem 226:112282
34. Kaky KM, Sayyed MI (2024) The radiation shielding parameters of a standard silica glass system. Silicon 16(3):1197–1203
35. Knoll GF (2010) Radiation detection and measurement. Wiley
36. Mudahar GS, Modi S, Makhan S (1991) Total and partial mass attenuation coefficients of soil as a function of chemical composition. Int J Radiation Appl Instrum Part Appl Radiation Isot 42(1):13–18
37. Medhat M (2012) Study of the mass attenuation coefficients and effective atomic numbers in some gemstones. J Radioanal Nucl Chem 293(2):555–564
38. Pires LF, Leite WC, Brinatti AM, Saab SC (2019) Radiation attenuation properties based on the quantification of soil components using the Rietveld Method. Results Phys 12:2009–2011
39. Camargo MA, Kodum KS, Pires LF (2021) How does the soil chemical composition affect the mass attenuation coefficient? A study using computer simulation to understand the radiation-soil interaction processes. Braz J Phys 51(6):1775–1783
40. Akça B, Erzeneoğlu SZ (2014) The mass attenuation coefficients, electronic, atomic, and molecular cross sections, effective atomic numbers, and electron densities for compounds of some biomedically important elements at 59.5 keV. Sci Technol Nuclear Installations 2014(1):901465

41. Lan, G., Liu, C., Wang, H., Tang, W., Wu, X., Yang, H., … Li, Q. (2021). The effect of land use change and soil redistribution on soil organic carbon dynamics in karst graben basin of China. Journal of Soils and Sediments, 21(7), 2511–2524.
42. Edem ID, Opara-Nadi OA, Ijah CJ (2012) Effects of biomass burning on soil properties and air quality under slash-and-burn agriculture. Agriculture 52:11555–11564
43. Hila, F. C., Dicen, G. P., Javier-Hila, A. M. V., Asuncion-Astronomo, A., Guillermo,N. R. D., Rallos, R. V., … Amorsolo Jr, A. V. (2021). Determination of photon shielding parameters for soils in mangrove forests.
44. Kumar TK, Venkataratnam S, Reddy KV (1996) Effective atomic number studies in clay minerals for total photon interaction in the energy region 10 keV–10 MeV. Radiat Phys Chem 48(6):707–710
45. Zhang, Q., Guo, Y., Bai, H., Gu, Y., Xu, Y., Zhao, J., … Liu, J. (2018). Determination of effective atomic numbers and mass attenuation coefficients of samples using in-situ energy-dispersive X-ray fluorescence analysis. X-Ray Spectrometry, 47(1), 4–10.
46. Un A, Sahin Y (2012) Determination of mass attenuation coefficients, effective atomic numbers, effective electron numbers and kermas for Earth and Martian soils. Nucl Instrum Methods Phys Res Sect B 288:42–47

# Figures

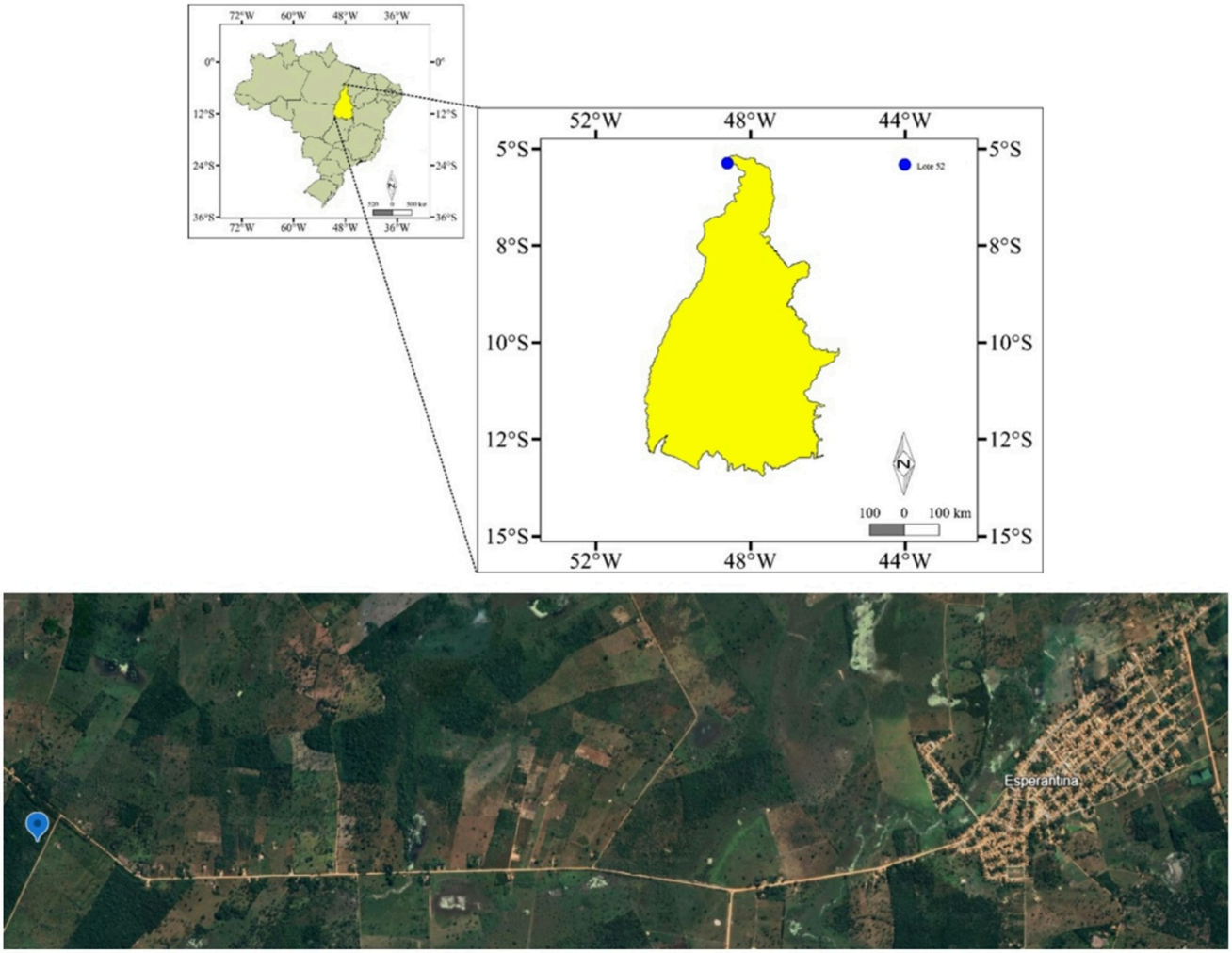



**Figure 1**

Map of Brazil showing the location of the state of Tocantins and the municipality of Esperantina. The satellite image from Google Earth shows the city of Esperantina and the location (pin) where the samples were collected.

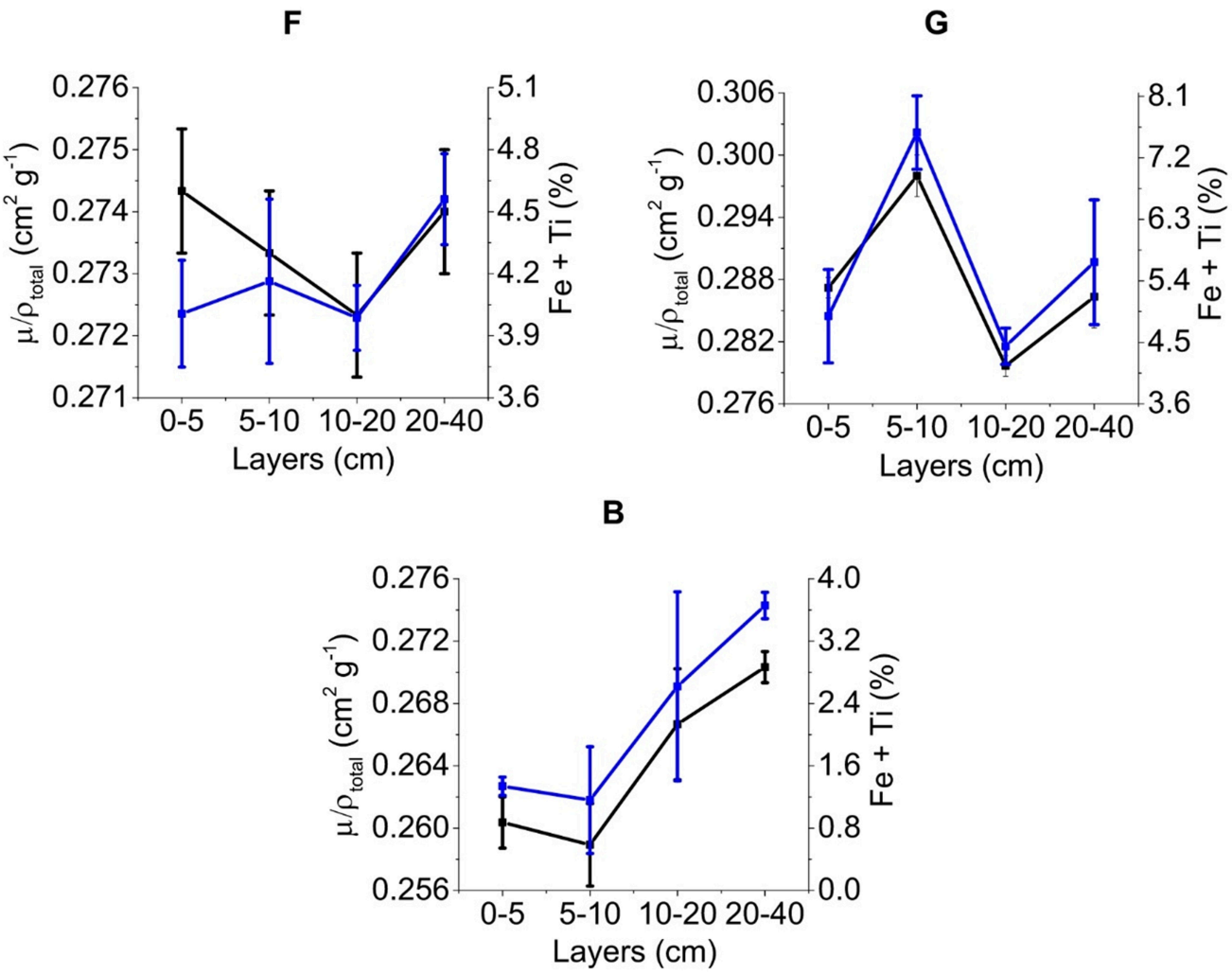



**Figure 2**

Trend in the variation of the mass attenuation coefficient (μ/ρ) (black line) and the $Fe_2O_3$+$TiO_2$oxide (blue line), as a function of soil depth (0–5, 5–10, 10–20, 20–40 cm) for forest (F), grassland (G), and biomass burning (B). The vertical lines indicate the standard deviation from the mean.

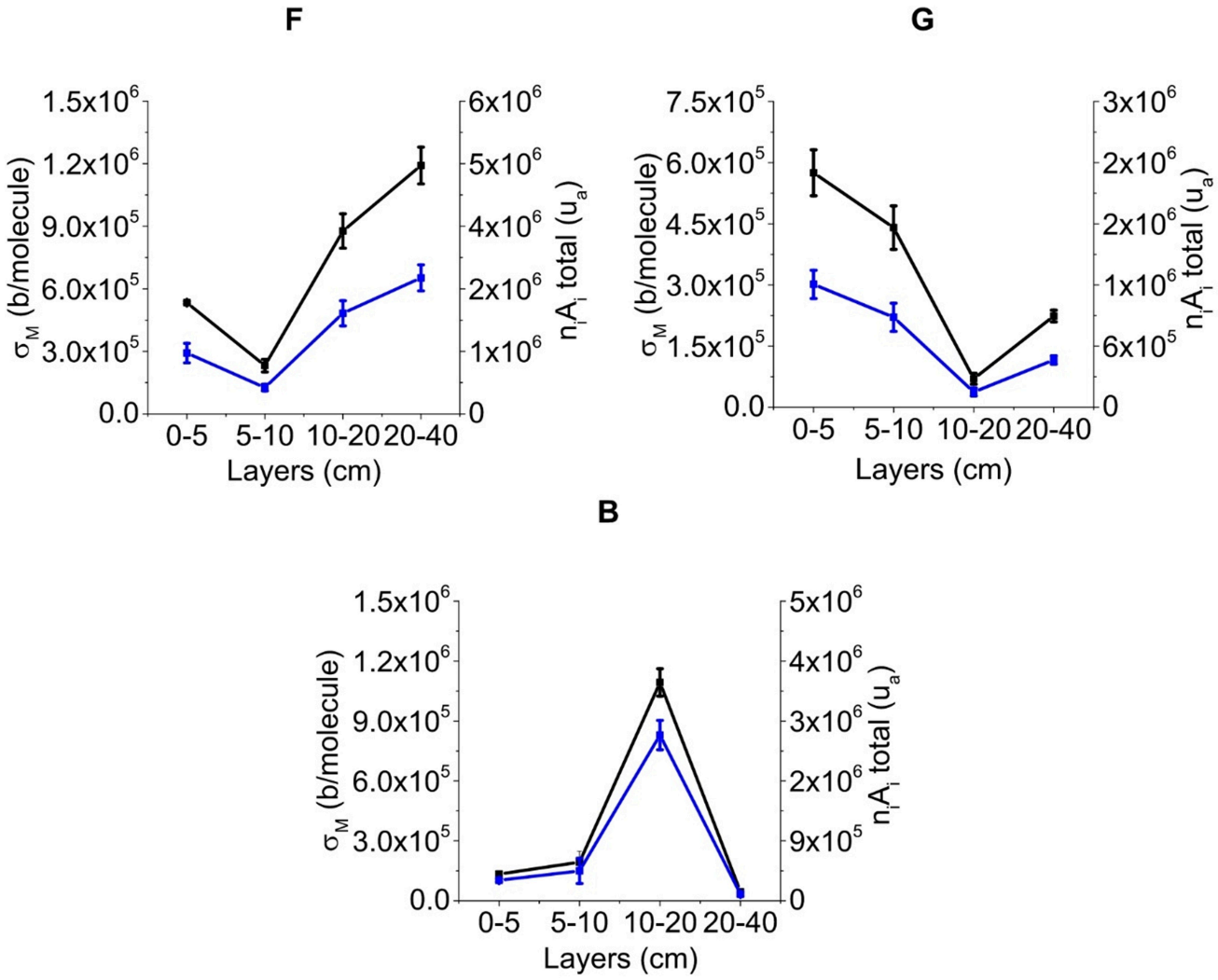



**Figure 3**

Trend in the variation of the molecular cross-section ($\sigma_M$) (blue line) and the total molecular weight of the compound ($n_iA_i$) (black line), as a function of soil depth (0–5, 5–10, 10–20, 20–40 cm) for forest (F), grassland (G), and biomass burning (B). The vertical lines indicate the standard deviation from the mean.

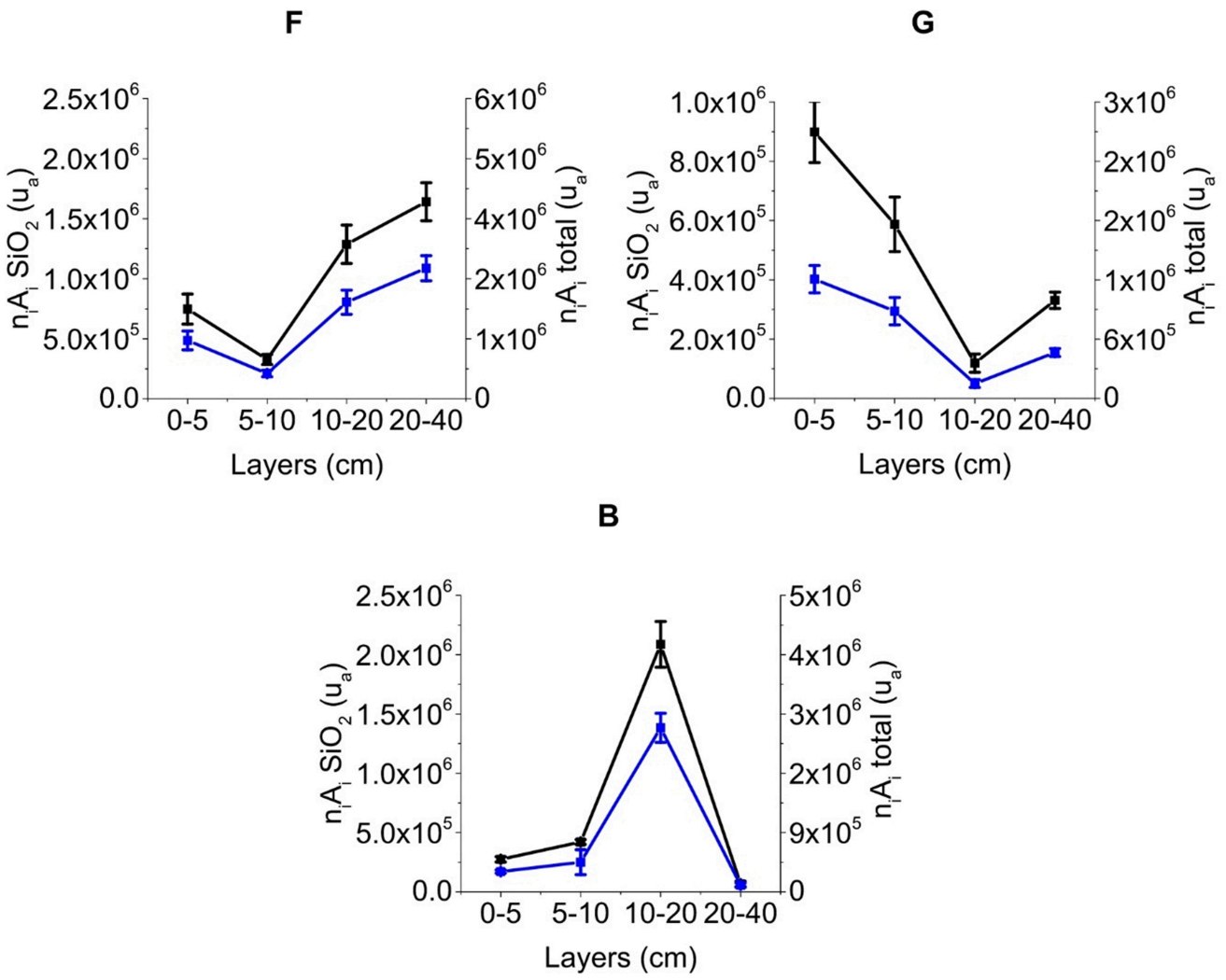



**Figure 4**

Trend in the variation of the total molecular weight of the compound ($n_iA_i$) (black line) and the $n_iA_i$ of $SiO_2$ (blue line) as a function of soil depth (0–5, 5–10, 10–20, 20–40 cm) for forest (F), grassland (G), and biomass burning (B). The vertical lines indicate the standard deviation from the mean.

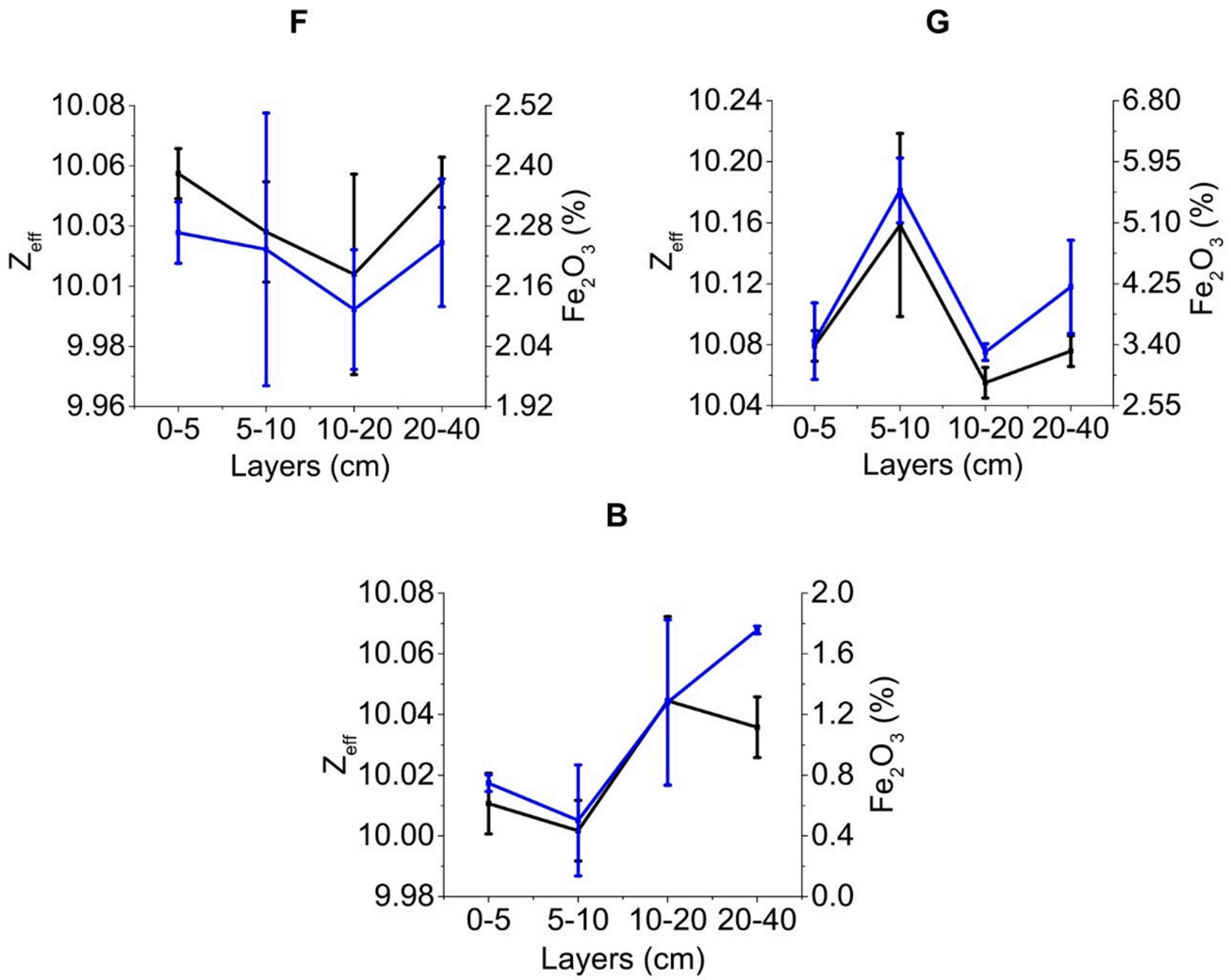



**Figure 5**

Trend in the variation of the effective atomic number ($Z_{eff}$) (black line) and the amount of $Fe_2O_3$ (blue line) as a function of soil depth (0–5, 5–10, 10–20, 20–40 cm) for forest (F), grassland (G), and biomass burning (B). The vertical lines indicate the standard deviation from the mean.

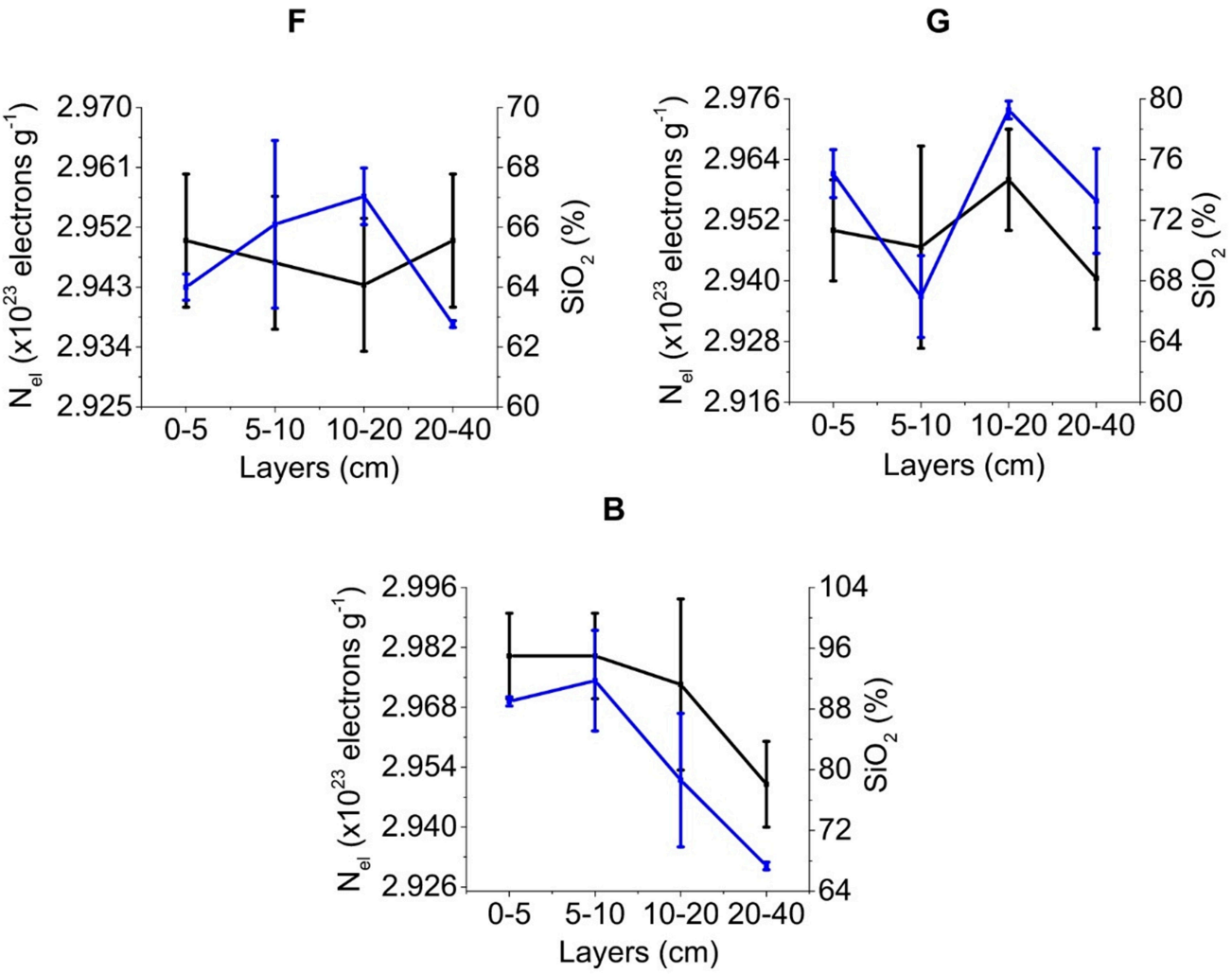



**Figure 6**

Trend in the variation of the electron density ($N_{el}$) (black line) and the amount of $SiO_2$ (blue line) as a function of soil depth (0–5, 5–10, 10–20, 20–40 cm) for forest (F), grassland (G), and biomass burning (B). The vertical lines indicate the standard deviation from the mean.